

www.acsanm.org Article

Single-Step Nonthermal Plasma Synthesis of Water-Soluble and Near-Infrared-Emitting Si Quantum Dots for Bioimaging Applications

Yeonjoo Lee, Mihee Kim, Jinkyoung Yoo, James H. Werner, and Uwe Kortshagen*



Cite This: ACS Appl. Nano Mater. 2024, 7, 21728-21734



ACCESS I

III Metrics & More

Article Recommendations

s Supporting Information

ABSTRACT: We present a single-step nonthermal plasma method for the synthesis of near-infrared (NIR)-emitting and water-soluble Si quantum dots (QDs) for bioimaging applications. Oxygen gas and water vapor were introduced together with acrylic acid (AA) into the afterglow region of the synthesis plasma leading to the surface functionalization of the upstream synthesized Si QDs. The simultaneous surface oxidation and ligand grafting enabled solubility and colloidal stability of the Si QDs in water, as evidenced by strongly reduced hydrodynamic diameters. Aged Si QDs in water emitted NIR photoluminescence (PL) at around 830 nm. The PL quantum yield of the Si QDs in water increased over time from initially undetectable to ~30% after 8 days. Cell viability tests showed that >70% of 3T3 cells survived for 24 h at a



concentration of 200 μ g/mL of oxidized AA grafted Si QDs. The water solubility, NIR emission with a high quantum yield, and cell viability make the Si QDs promising for bioimaging applications.

KEYWORDS: nonthermal plasma synthesis, silicon quantum dots, water-soluble nanocrystals, photoluminescence, cell viability, bioimaging

1. INTRODUCTION

Fluorescence bioimaging is an established and powerful noninvasive imaging technique providing real-time, high-contrast and high-resolution information. Recently, fluorescence bioimaging in the near-infrared (NIR) region has garnered attention because it significantly reduces the influence of autofluorescence, absorption and scattering by tissue, skin, fat and blood. NIR windows at 650–950 and 1000–1400 nm allow deep tissue penetration, improving image quality.

Silicon quantum dots (Si QDs) are desirable among fluorescent bioimaging probes for NIR imaging. In contrast to organic dyes, the emission of Si QDs is tunable within redto-NIR spectral range⁵ with high photoluminescence quantum yield (PLQY) and long-lived photoluminescence (PL) decay.⁶ In contrast, organic dyes emit in the ultraviolet (UV)-visible range with low PLQY and short lifetimes.⁷ The longer PL lifetime enables enhanced image contrast by gating out fast autofluorescence photons from cells, tissues, and others.^{2,8} Moreover, the large Stokes shift of Si QDs prevents reabsorption of the emitted light, enhancing sensitivity.^{7,9} In contrast to many other semiconductor QDs, Si QDs exhibit lower toxicity than heavy metal-based II-IV and III-V QDs. 10,11 The biocompatibility 12 and biodegradability 13 of Si QDs are also advantageous; Si QDs are decomposed into silicic acid in the body and excreted in urine.¹³

For bioimaging applications, Si QDs need to be water-soluble. To date, water-soluble Si QDs have been prepared mainly by multistep methods, which comprise the synthesis of pristine Si QDs and the subsequent processing to form hydrophilic surfaces. Postprocessing methods to impart hydrophilicity on Si QDs include the formation of surface oxides^{8,9} and the surface functionalization with polar ligands, such as amines, ^{14,15} carboxylic acids, ^{16–20} polyethylene glycol (PEG) groups, ^{21–24} and biomolecules such as amino acids, proteins, and sugars. ^{25–27}

In contrast to previous multistep methods to solubilize Si QDs, here we present a single-step nonthermal plasma synthesis method for Si QD synthesis and solubilization in water. This work builds on our previous work to synthesize and surface functionalize Si QDs in a single step in a nonthermal plasma. ^{22,28–30} In this single-step method, hydrogen-terminated Si QDs are first synthesized in the plasma region of a continuous flow plasma reactor, and then surface

Received: June 28, 2024
Revised: August 30, 2024
Accepted: September 2, 2024
Published: September 10, 2024





functionalized further downstream in the plasma afterglow. This single-step synthesis method saves time and energy in producing functionalized Si QDs, generating less chemical waste compared to other solution-based methods. Furthermore, it provides narrow size and shape distributions as well as crystallinity of the Si QDs.³¹

Water-soluble Si QDs were previously prepared by first synthesizing acrylic acid (AA) grafted Si QDs (AA-Si QDs) using the single-step method discussed above and an then reacting these QDs with PEG for 72 h. 22 The post-treatment of the gas-phase produced AA-Si QDs was required because the surface coverage of Si QDs with AA ligands achieved via gas phase functionalization is typically less than 30%, which is significantly lower than that of Si QDs functionalized in the liquid phase. 32 Based on this prior work, we hypothesize that the water solubility of Si QDs synthesized by single-step nonthermal plasma synthesis can be significantly improved by increasing the Si QDs' surface coverage with hydrophilic surface groups.

Here, we report a single-step synthesis of NIR-emitting and water-soluble Si QDs by combining in-flight AA functionalization and simultaneous surface oxidation in one nonthermal plasma reactor. An oxidizer, either oxygen (O_2) or water vapor (H_2O) , was introduced simultaneously with the AA ligands into the afterglow of the nonthermal synthesis plasma. The C=C bond in AA reacts with Si-H bonds on the Si QD surfaces, aided by plasma, resulting in the formation of Si-C bonds. Simultaneously, O_2 or H_2O replaces hydrophobic Si-H bonds with hydrophilic Si-O bonds. Since the replacement of H atoms with O atoms can naturally occur in ambient air, the plasma-assisted process likely enhances the removal of surface hydrogen atoms. To evaluate the suitability of the so-produced Si QDs for potential bioimaging applications, cell viability tests were conducted with 3T3 cells.

2. EXPERIMENTAL SECTION

2.1. Synthesis of Water-Soluble Si QDs. Figure 1 shows a schematic of the synthesis of oxidized AA-Si QDs in a single-step plasma reactor. The reactor was based on the nonthermal plasma reactor developed for the fast synthesis of silicon nanocrystals described in ref 33. Hydrogen-terminated Si QDs (H–Si QDs) are synthesized in the intense plasma region near the copper ring electrodes; the surface functionalization process follows downstream in the plasma afterglow region with reduced plasma density. AA and oxidizer molecules are injected into the afterglow region through a side arm with Ar carrier gas. After the surface functionalization, Si QDs pass through a slit-shaped orifice and are collected on a substrate by impaction. The AA-Si QDs oxidized with water vapor and O₂ are referred to as AA-H₂O–Si QDs and AA-O₂–Si QDs, respectively.

The quartz tube utilized had two different diameters; the upstream part had an outer diameter (OD) of 0.375 in., while the downstream part was 1 in. in OD. The wall thickness of the 1-in. section was 0.13 in. To generate the plasma, radio frequency (RF) power was applied through an impedance matching network to a pair of copper ring electrodes at 13.56 MHz and 60 W. The reflected power was kept lower than 2 W. Here power refers to the power supplied by the RF power supply, the power actually coupled into the plasma is expected to be lower. The position of the ring electrodes was 3–4 cm upstream of the afterglow gas injection points.

The reactor pressure ranged from 2.6 to 2.8 torr, measured at the top of the reactor tube. The flow rates of silane and the main Ar gas to dilute silane were 14 and 30 sccm, respectively. AA or AA/H_2O solution in a bubbler was delivered with 50 sccm of Ar through a separate line. The bubbler pressure was adjusted by a needle valve at the bubbler downstream, and the typical bubbler pressure was around 25 mtorr with the valve fully opened. The glass tube of the bubbler

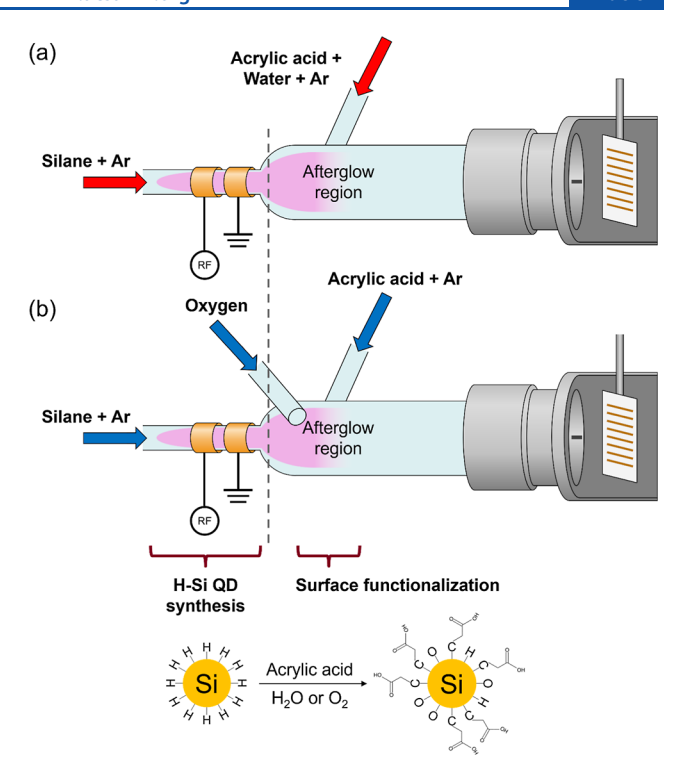


Figure 1. Schematics of nonthermal plasma reactors for the all-gasphase synthesis of (a) AA-H₂O-Si QD and (b) AA-O₂-Si QD.

was covered with aluminum foil to prevent the polymerization of AA. Si QDs were collected downstream of the reactor by inertial impaction, passing through an orifice. The mass yield was $0.3~\mathrm{mg/min}$.

2.2. Material Characterization. X-ray diffraction (XRD), Fourier transform infrared (FTIR) spectroscopy, and dynamic light scattering (DLS) were conducted for the characterization of the Si QDs. XRD patterns were obtained using a D8 Discover diffractometer (Bruker, Billerica, MA) with a Co X-ray source. The XRD samples were prepared by deposition on a glass substrate as a pile. An Alpha spectrometer (Bruker, Billerica, MA) with a diffuse reflectance infrared Fourier transform (DRIFT) module was used to perform FTIR spectroscopy in a glovebox under a nitrogen atmosphere. Samples for the DRIFT module were prepared by directly depositing them on a piece of aluminum-coated Si wafer. DLS measurements used a Nanoflex DLS nanoparticle size analyzer (Microtrac, York, PA). All DLS samples were prepared with a concentration of 1.5 mg/mL.

Optical characteristics of the Si QDs were studied by PLQY and time-resolved PL (TRPL) measurements. A USB2000 spectrometer (OceanOptics, Orlando, FL) was used to collect the PL spectrum with an integrating sphere. The excitation source was an LED diode with a wavelength of 396 nm mounted in the integrating sphere. For TRPL, a DeltaFlex TCSPC Lifetime Fluorometer (Horiba, Irvine, CA) was employed with an excitation source of a 407 nm laser, and a delay time of 13 μs .

2.3. Cell Culture and Cell Viability Measurement. All Si QDs were aged in DI water for at least 1 week to be NIR-emitting before sample preparation. The cell viability tests were conducted three times on three different dates using three replicates of each QD type (AA-O₂- and AA-H₂O-Si QDs) and concentrations (100, 200, and 400 μ g/mL). When cell confluency reached ~50–60%, Si QDs were added to 3T3 cells and incubated for 24 h.

NIH 3T3 cells (CRL-1658; AmericanType Culture Collection, Manassas, VA) were cultured in Dulbecco's modified Eagle medium (DMEM), 10% fetal bovine serum, and 1% penicillin/streptomycin at 37 $^{\circ}$ C humidified atmosphere of 5% CO₂. Cells were routinely passaged before reaching 80% confluency by washing twice with

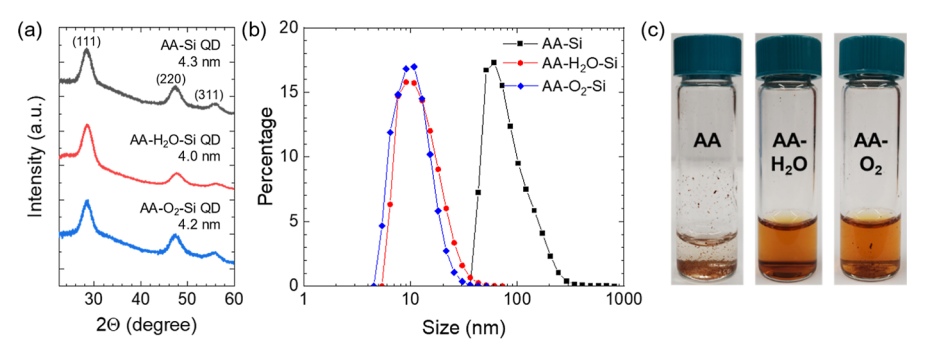


Figure 2. (a) XRD patterns of AA-Si, AA-H₂O-Si, AA-O₂-Si QDs. (b) Hydrodynamic diameters of functionalized Si QDs dispersed in water at 1.5 mg/mL. (c) Photographs showing the results after adding water to the as-synthesized AA-Si, AA-O₂-Si, and AA-H₂O-Si QDs, followed by mixing by hand-shaking the vials.

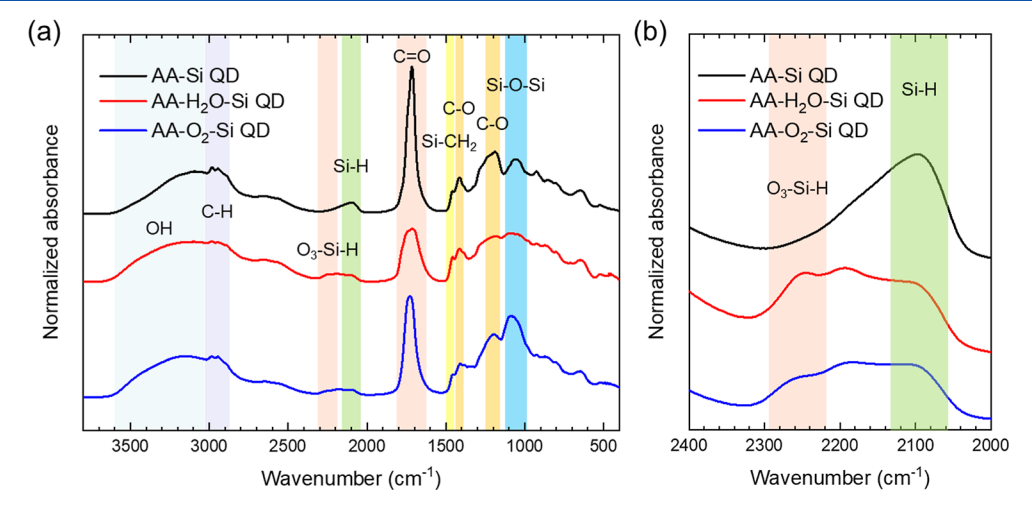


Figure 3. (a) FTIR spectra of AA-Si, AA-H₂O-Si, and AA-O₂-Si QDs. (b) FTIR spectra focused on O₃-Si-H and Si-H bands.

Dulbecco's phosphate-buffered saline and then harvested with a 0.25% Trypsin solution. For cell viability measurements, approximately 1000 cells per well were seeded in a 96-well cell culture plate. After incubation at 37 °C in a humidified atmosphere with 5% CO₂ for 48 h, the culture medium was replaced with the Si QD solution. The composition of Si QD solution is 100 or 200 μ g Si QDs dissolved in phenol-red free culture medium (10% fetal bovine serum and 1% penicillin/streptomycin in FluoroBrite DMEM). After incubating cells with Si QD solution for 1 day at 37 °C humidified atmosphere of 5% CO₂. Si QD solution was carefully replaced with phenol-red free culture medium. 10 μ L of FastCounting solution was added to each well of the plate. After 4 h of incubation in the incubator, absorbance at 450 nm was measured using a Spark Cyto plate reader (TECAN, Baldwin Park, CA). Five replicates were made for control.

3. RESULTS AND DISCUSSION

Figure 2A shows the XRD patterns of AA-Si QDs, AA-H₂O-Si QDs, and AA-O₂-Si QDs. The XRD patterns for all three types of Si QDs show peaks at 28.4, 47.4, and 55.9°, corresponding to Si (111), (220), and (311) reflections, respectively.³⁵ The sizes of the Si QDs were estimated using a modified Scherrer's equation for nanocrystals based on the (220) peaks³⁶

$$d = \frac{3}{4} \times \frac{0.9\lambda}{w\cos\theta} \tag{1}$$

where d is the nanocrystal diameter, λ is the wavelength of the X-ray source, θ is one-half of the diffraction angle, and w is full width at half-maximum.

The estimated sizes of AA-Si QDs, AA- H_2O -Si QDs, and AA- O_2 -Si QDs are 4.3, 4.0, and 4.2 nm, respectively. The similar QD sizes for different oxidation treatments indicate that the oxygen and water vapor injections do not affect the Si QD core sizes.

Figure 2B shows the hydrodynamic diameters of AA-Si QDs, AA-H₂O-Si QDs, and AA-O₂-Si QDs measured by DLS in deionized (DI) water with a concentration of 1.5 mg/mL. The hydrodynamic diameters of AA-Si QDs, AA-H₂O-Si QDs, and AA-O₂-Si QDs are 81 \pm 34, 12 \pm 4.7, and 10 \pm 3.6 nm, respectively. The strong reduction of the Si QD hydrodynamic diameters with oxidizer injection indicates significantly reduced aggregation of these Si QDs in aqueous solution. The hydrodynamic diameters measured by DLS are typically larger than the actual particle sizes as determined by XRD. DLS measurements indicate not only the actual particle size but also contributions from surface ligands, surrounding solvent molecule layers, and any aggregates formed by the QDs. The discrepancies between XRD and DLS measurements are consistent with results for AA-Si QDs reported in ref 37.

The improvement of water solubility can be observed by adding DI water to as-synthesized Si QDs. Figure 2C shows the dispersion of AA-Si QDs, AA-H₂O-Si QDs, and AA-O₂-Si QDs in water. The AA-Si QDs were not readily dispersible in water. On the other hand, AA-H₂O-Si QDs and AA-O₂-Si QDs were easily dispersed in water by shaking the vials for a few seconds. Also, after dozens of minutes, precipitation was observed in the AA-Si QD solution, whereas the two samples

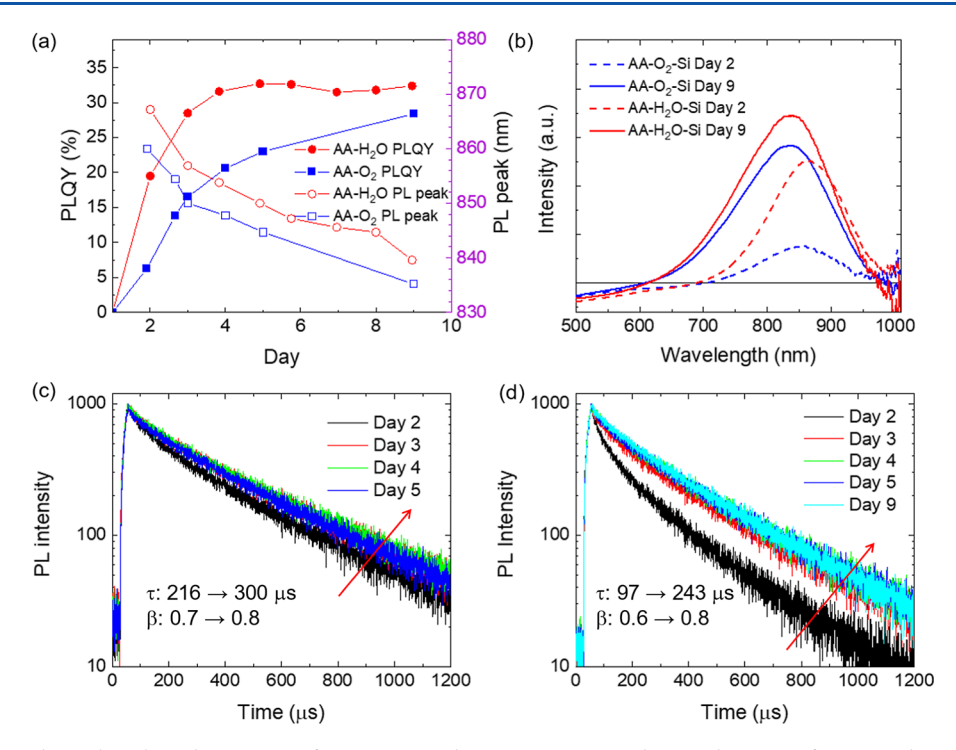


Figure 4. (a) PLQYs and wavelength peak positions of AA- O_2 -Si and AA- H_2O -Si QDs dispersed in water for 0 to 9 days. (b) PL spectra of AA- O_2 -Si and AA- H_2O -Si QDs on day 2 (dashed) and day 9 (solid) when the PLQY reached saturation in water. Time-resolved PL spectra of (c) AA- H_2O -Si QDs dispersed in water over 2 to 5 days and (d) AA- O_2 -Si QDs dispersed in water over 2 to 9 days.

treated with oxidizers remained stable without any precipitation for over one year.

The changes in surface species with the oxidizer injections were investigated by FTIR. Figure 3A shows the emergence of peaks in 2800–3000, 1700–1800, and 1450 cm⁻¹ spectral ranges, corresponding to C–H stretching, C=O stretching, and Si–CH₂ stretching modes, respectively. The AA functionalization induced the replacement of surface Si–H bonds with Si–C bonds. The increase in the Si–O–Si peaks (~1080 cm⁻¹) to relative to the C=O absorptions with oxidizer injection indicates the enhanced oxidation of the Si QD surfaces compared to the untreated AA-Si QDs. The emergence of the O₃–Si–H peak at 2200–2300 cm⁻¹ for the O₂ and H₂O treated samples, which is lacking for the untreated samples, as shown in Figure 3B, also indicates the enhanced surface oxidation of the Si QDs upon oxidizer injection. The peak is a surface oxidation of the Si QDs upon oxidizer injection.

The optical characteristics of the water-soluble Si QDs were characterized by time-integrated and time-resolved photoluminescence (PL) measurements. Figure 4A shows the PL peaks and the PLQY of AA-H₂O-Si QDs and AA-O₂-Si QDs over time in DI water. Initially, the PLQYs of the AA-H₂O-Si QDs and AA-O2-Si QDs were lower than the detection limit of the measurement setup. The PLQYs of the Si QDs increased over time when stored in water, as shown in Figure 4A. The PLQY of AA-H₂O-Si QDs reached a maximum value of ~32% after 4 days. Meanwhile, it took 9 days for the PLQY of AA-O₂-Si QDs to reach ~30%. While the PLQY of both oxidized AA-Si QD samples was rising, the PL peak wavelength continued to blueshift, as shown in Figure 4A, B. During the storage of the Si QDs in water, the PLOY rise and PL blueshift occurred concurrently, which can be attributed to the formation of an oxide shell that passivates nonradiative surface defects, such as dangling bonds, and leads to a reduction of the Si QD core size by reacting Si into silicon oxide at the QD surface. Some studies have reported improvements in PLQY for surface-oxidized Si QDs due to similar mechanisms.^{40–42} While in the present study the functionalization with AA and oxidizers provided water solubility, it is likely that residual surface defects are suppressing radiative recombination in the Si QDs. Therefore, the growth of the oxide layer contributes to the enhancement of PLQY by suppressing the residual surface defects.

While the Si QD oxidation slows down after 9 days, it does not completely stop. After one year, the oxidized AA-Si QDs, which were stored in water, exhibited red PL emission at \sim 600 nm. In cases of wet oxidation, water molecules can penetrate the silicon oxide shell, even when the Si QDs are protected by capping agents. Therefore, if the Si QDs are stored in an aqueous solution for an extended period, they are expected to undergo thorough oxidation and eventually dissolve into silicic acid (Si(OH)₄).

The PL enhancements were further investigated by TRPL measurements. Figure 4C,D show the PL decay profiles of AA-H₂O-Si QDs and AA-O₂-Si QDs. The PL decay can be described by a stretched-exponential decay model I = $I_0 \exp(-(t/\tau)^{\beta})$, where τ is PL lifetime and β is dispersion factor. 43 The radiative decay dynamics of Si QDs is affected by surface oxidation in water. As shown in Figure 4C,D, for both oxidizers τ increased together over time as the PLQY also rose. The lifetimes were in the \sim 100–300 μ s range, which is typical for PL originating from Si QD cores. 44-46 The increases in aucan be explained by surface passivation through oxide shell formation over time. The reduction of the probability of nonradiative recombination via surface passivation induces an increase in τ toward the radiative recombination lifetime.^{44–} The increase in β also reflects effects of the surface passivation through oxide shell formation. Stretched exponential behavior with β < 1 has been observed both in solid state samples of Si QDs, 44 where it is often associated with exciton transfer, as well as colloidal Si QD samples, 47 where this effect should play

less of a role. While the nature of the origin of the stretched exponential decay remains under discussion, β approaching 1 is usually associated with improved optical properties of Si QDs. ⁴⁷

The oxidized AA-Si QDs exhibit good water solubility, small hydrodynamic diameters, and NIR PL with long lifetimes. These properties indicate that the water-soluble Si QDs may have a good potential for bioimaging applications, for which low toxicity is also required for bioimaging applications. We evaluated the cell cytotoxicity of the oxidized AA-Si QDs using 3T3 cells. Figure 5 shows the cell viability of 3T3 cells in the

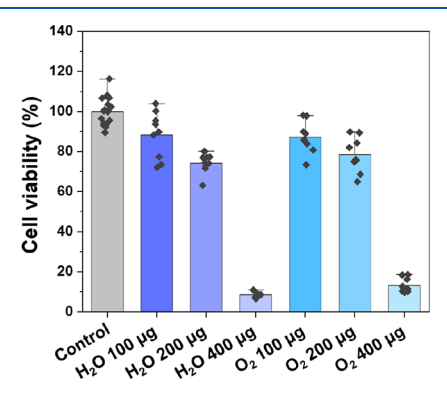


Figure 5. 3T3 cell viability of AA- H_2O -Si QDs and AA- O_2 -Si QDs incubated in biological media with three different concentrations of 100, 200, and 400 μ g/mL for 24 h.

presence of AA-H₂O–Si QDs and AA-O₂–Si QDs at different QD concentrations. For 100 and 200 μ g/mL of AA-H₂O–Si QDs and AA-O₂–Si QDs, the cell viability is higher than 70%, whereas most of the cells were dead at 400 μ g/mL. Compared to a previous study with poly-AA-Si nanoparticles (PAA-Si NPs) and 3T3 cells, ^{37,48} the viability of AA-O₂–Si and AA-H₂O–Si QDs is lower; in the PAA-Si NP study, the viability remained around 100% for 24 h up to 200 μ g/mL. Nevertheless, the half-maximal inhibitory concentration IC₅₀ values of the oxidized AA-Si QDs are higher than 200 mg/L, which is significantly larger than a typical IC₅₀ value of 25 mg/L for cadmium-containing QDs. ⁴⁹ Therefore, our oxidized AA-Si QDs can be considered relatively nontoxic for bioimaging applications.

Our Si QDs also showed a larger toxicity than a previous study using 10-undecenoic acid functionalized Si QDs and HeLa cells. While our results are not directly comparable to ref 50 due to the different cell types, the difference in toxicity may also be the results of different ligands. The 10-undecenoic acid (CH₂=CH(CH₂)₈COOH) ligands used in ref 50 are bulkier than AA (CH₂=CHCOOH) used here. The larger size of 10-undecenoic acid likely results in fewer ligands on the Si QD surface due to steric hindrance. Since both 10-undecenoic acid and AA have one carboxylic acid group, it can be inferred that our Si QDs may have a higher concentration of carboxylic acid groups. This could lead to more acidic conditions near the cells, which may cause higher toxicity.

The main advantage of our water-soluble Si QDs lies in the simplicity of the synthesis method. The process requires less time, energy, and fewer chemicals compared to other water-soluble Si QD synthesis methods. For instance, other methods often require HF treatment to remove oxides and terminate Si QDs with hydrogen before functionalizing them with AA. Additionally, hours of UV irradiation are typically needed to

induce the reaction between organic molecules and hydrogenterminated Si surfaces. ^{17,37} In solution-phase functionalization, postprocessing steps such as purification, ⁵⁰ filtering, ²² or dialysis ¹⁷ are necessary to separate the Si QDs and remove residual reactants. Furthermore, Si QDs are usually synthesized with hydrogen- or halogen-terminated surfaces, which are hydrophobic, making it more challenging to achieve water solubility compared to solubility in nonpolar solvents.

We emphasize that our simple and rapid synthesis method effectively addresses these challenges, enabling efficient functionalization without the need for extensive postprocessing. This approach is more significant than improvements in cell cytotoxicity alone. Additionally, our Si QDs feature carboxylic groups, allowing easy decoration with molecules containing amine groups, demonstrated in ref 51. This capability not only enhances cell viability but also broadens the potential biological applications of our water-soluble Si QDs. 51

4. CONCLUSION

For producing Si QDs suitable for bioimaging applications, the aim is to synthesize Si QDs with NIR PL and peak PL wavelengths >750 nm, corresponding to 3-5 nm-sized Si cores, PLQYs >20% in water, and hydrodynamic diameters <20 nm. We developed a single-step nonthermal plasma synthesis of water-soluble, NIR-emitting Si QDs via simultaneous oxidation and surface functionalization. The water solubility of AA-Si QDs was enhanced by adding oxidizers, either oxygen or water vapor, into the afterglow of the synthesis plasma. The wavelength of the PL was in the range of 800-900 nm, which is suitable for bioimaging applications. After aging in water dispersion for 5-9 days, the PLQY increased by up to ~30% with hydrodynamic diameters of 10 and 12 nm. The PLQY is favorable compared to other watersoluble Si QDs reported in previous studies, as shown in Table S1 in the Supporting Information. Additionally, the PL lifetime was $\sim 200 \mu s$, which is at least 100 times longer than that of conventional fluorescence bioimaging probes. The cell viability tests showed the suitability of oxidized AA-Si QDs as potential bioimaging probes providing monitoring times of 24 h at concentrations of up to 200 μ g/mL. The single-step plasma synthesis of hydrophilic Si QDs discussed here is advantageous in terms of energy and time consumption by eliminating postprocessing generally required in the synthesis of watersoluble Si QDs.

ASSOCIATED CONTENT

Supporting Information

The Supporting Information is available free of charge at https://pubs.acs.org/doi/10.1021/acsanm.4c03643.

PL peak wavelengths and QYs of various studies of water-soluble Si QDs for bioimaging applications (PDF)

AUTHOR INFORMATION

Corresponding Author

Uwe Kortshagen – Department of Mechanical Engineering, University of Minnesota, Minneapolis, Minnesota 55455, United States; ⊚ orcid.org/0000-0001-5944-3656; Email: korts001@umn.edu

Authors

Yeonjoo Lee — Department of Mechanical Engineering, University of Minnesota, Minneapolis, Minnesota 55455, United States; oorcid.org/0000-0003-2096-5160

Mihee Kim — Center for Integrated Nanotechnologies, Los Alamos National Laboratory, Los Alamos, New Mexico 87545, United States; oorcid.org/0000-0002-6258-7287

Jinkyoung Yoo — Center for Integrated Nanotechnologies, Los Alamos National Laboratory, Los Alamos, New Mexico 87545, United States; orcid.org/0000-0002-9578-6979

James H. Werner — Center for Integrated Nanotechnologies, Los Alamos National Laboratory, Los Alamos, New Mexico 87545, United States; orcid.org/0000-0002-7616-8913

Complete contact information is available at: https://pubs.acs.org/10.1021/acsanm.4c03643

Author Contributions

Y.L. performed the QD synthesis and the measurements. M.K. and Y.L. conducted the cell viability test. J.W. was involved in discussions for the cell viability test. J.Y. arranged and planned experiments conducted at the Los Alamos National Laboratory. Y.L. and J.Y. wrote the manuscript. U.K. was involved in the conceptualization of experiments at the University of Minnesota, supervision of research, acquisition of funding, and editing the manuscript. All authors have given approval to the final version of the manuscript.

Funding

This work was supported by the National Institute of Health under Award R01DA045549. XRD, XPS, and TEM were carried out in the Characterization Facility, University of Minnesota, which receives partial support from NSF through the MRSEC program Award DMR-2011401. Portions of this work were conducted in the Minnesota Nano Center, which is supported by the National Science Foundation through the National Nano Coordinated Infrastructure (NNCI) Network under Award ECCS-2025124.

Notes

The authors declare no competing financial interest.

ACKNOWLEDGMENTS

A part of the research was financially supported by the Laboratory Directed Research and Development program of Los Alamos National Laboratory (20230256ER). This work was partly performed at CINT, a U.S. Department of Energy, office of Basic Energy Sciences User Facility at Los Alamos National Laboratory (Contract 89233218CNA000001) and Sandia National Laboratories (Contract DE-NA-0003525).

ABBREVIATIONS

XRD X-ray diffraction

FTIR Fourier-transform infrared

DRIFT diffuse reflectance DLS dynamic light scattering PL photoluminescence

PLQY photoluminescence quantum yield TRPL time-resolved photoluminescence fwhm full width at half-maximum XPS X-ray photoelectron spectroscopy

UV ultraviolet

REFERENCES

- (1) Li, C.; Wang, Q. Challenges and opportunities for intravital near-infrared fluorescence imaging technology in the second transparency window. ACS Nano 2018, 12 (10), 9654–9659.
- (2) Gil, H. M.; Price, T. W.; Chelani, K.; Bouillard, J.-S. G.; Calaminus, S. D.; Stasiuk, G. J. NIR-quantum dots in biomedical imaging and their future. *iScience* **2021**, *24* (3), 102189.
- (3) Zhang, Y.; Cai, N.; Chan, V. Recent Advances in Silicon Quantum Dot-Based Fluorescent Biosensors. *Biosensors* **2023**, *13* (3), 311.
- (4) Smith, A. M.; Mancini, M. C.; Nie, S. Second window for in vivo imaging. *Nat. Nanotechnol.* **2009**, *4* (11), 710–711.
- (5) Kang, Z.; Liu, Y.; Tsang, C. H. A.; Ma, D. D. D.; Fan, X.; Wong, N. B.; Lee, S. T. Water-soluble silicon quantum dots with wavelength-tunable photoluminescence. *Adv. Mater.* **2009**, *21* (6), 661–664.
- (6) Beri, D. Silicon quantum dots: surface matter, what next? *Mater. Adv.* **2023**, *4*, 3380–3398.
- (7) Resch-Genger, U.; Grabolle, M.; Cavaliere-Jaricot, S.; Nitschke, R.; Nann, T. Quantum dots versus organic dyes as fluorescent labels. *Nat. Methods* **2008**, *5* (9), 763–775.
- (8) Pons, T.; Bouccara, S.; Loriette, V.; Lequeux, N.; Pezet, S.; Fragola, A. In vivo imaging of single tumor cells in fast-flowing bloodstream using near-infrared quantum dots and time-gated imaging. ACS Nano 2019, 13 (3), 3125–3131.
- (9) Meinardi, F.; Ehrenberg, S.; Dhamo, L.; Carulli, F.; Mauri, M.; Bruni, F.; Simonutti, R.; Kortshagen, U.; Brovelli, S. Highly efficient luminescent solar concentrators based on earth-abundant indirect-bandgap silicon quantum dots. *Nat. Photonics* **2017**, *11* (3), 177–185.
- (10) Pramanik, S.; Hill, S. K.; Zhi, B.; Hudson-Smith, N. V.; Wu, J. J.; White, J. N.; McIntire, E. A.; Kondeti, V. S. S. K.; Lee, A. L.; Bruggeman, P. J.; Kortshagen, U. R.; Haynes, C. L. Comparative toxicity assessment of novel Si quantum dots and their traditional Cd-based counterparts using bacteria models Shewanella oneidensis and Bacillus subtilis. *Environ. Sci.: Nano* **2018**, *5* (8), 1890–1901.
- (11) Liu, J.; Erogbogbo, F.; Yong, K.-T.; Ye, L.; Liu, J.; Hu, R.; Chen, H.; Hu, Y.; Yang, Y.; Yang, J.; et al. Assessing clinical prospects of silicon quantum dots: studies in mice and monkeys. *ACS Nano* **2013**, *7* (8), 7303–7310.
- (12) Bimbo, L. M.; Sarparanta, M.; Santos, H. A.; Airaksinen, A. J.; Makila, E.; Laaksonen, T.; Peltonen, L.; Lehto, V.-P.; Hirvonen, J.; Salonen, J. Biocompatibility of thermally hydrocarbonized porous silicon nanoparticles and their biodistribution in rats. *ACS Nano* **2010**, *4* (6), 3023–3032.
- (13) Park, J.-H.; Gu, L.; Von Maltzahn, G.; Ruoslahti, E.; Bhatia, S. N.; Sailor, M. J. Biodegradable luminescent porous silicon nanoparticles for in vivo applications. *Nat. Mater.* **2009**, 8 (4), 331–336.
- (14) Atkins, T. M.; Louie, A. Y.; Kauzlarich, S. M. An efficient microwave-assisted synthesis method for the production of water soluble amine-terminated Si nanoparticles. *Nanotechnology* **2012**, 23 (29), 294006.
- (15) Warner, J. H.; Rubinsztein-Dunlop, H.; Tilley, R. D. Surface morphology dependent photoluminescence from colloidal silicon nanocrystals. *J. Phys. Chem. B* **2005**, *109* (41), 19064–19067.
- (16) Clark, R. J.; Dang, M. K.; Veinot, J. G. Exploration of organic acid chain length on water-soluble silicon quantum dot surfaces. *Langmuir* **2010**, 26 (19), 15657–15664.
- (17) Sato, S.; Swihart, M. T. Propionic-acid-terminated silicon nanoparticles: synthesis and optical characterization. *Chem. Mater.* **2006**, *18* (17), 4083–4088.
- (18) He, Y.; Kang, Z.-H.; Li, Q.-S.; Tsang, C. H. A.; Fan, C.-H.; Lee, S.-T. Ultrastable, highly fluorescent, and water-dispersed silicon-based nanospheres as cellular probes. *Angew. Chem., Int. Ed.* **2009**, *48* (1), 128–132.
- (19) Yu, Y.; Hessel, C. M.; Bogart, T. D.; Panthani, M. G.; Rasch, M. R.; Korgel, B. A. Room temperature hydrosilylation of silicon nanocrystals with bifunctional terminal alkenes. *Langmuir* **2013**, 29 (5), 1533–1540.
- (20) Fan, J.-W.; Vankayala, R.; Chang, C.-L.; Chang, C.-H.; Chiang, C.-S.; Hwang, K. C. Preparation, cytotoxicity and in vivo bioimaging

- of highly luminescent water-soluble silicon quantum dots. *Nano-technology* **2015**, *26* (21), 215703.
- (21) Islam, M. A.; Sinelnikov, R.; Howlader, M. A.; Faramus, A.; Veinot, J. G. Mixed surface chemistry: an approach to highly luminescent biocompatible amphiphilic silicon nanocrystals. *Chem. Mater.* **2018**, 30 (24), 8925–8931.
- (22) Li, Z.; Mahajan, A.; Andaraarachchi, H. P.; Lee, Y.; Kortshagen, U. R. Water-soluble luminescent silicon nanocrystals by plasma-induced acrylic acid grafting and PEGylation. *ACS Appl. Bio Mater.* **2022**, *5* (1), 105–112.
- (23) Maurice, V.; Slostowski, C.; Herlin-Boime, N.; Carrot, G. Polymer-grafted silicon nanoparticles obtained either via peptide bonding or click chemistry. *Macromol. Chem. Phys.* **2012**, *213* (23), 2498–2503.
- (24) Romano, F.; Angeloni, S.; Morselli, G.; Mazzaro, R.; Morandi, V.; Shell, J. R.; Cao, X.; Pogue, B. W.; Ceroni, P. Water-soluble silicon nanocrystals as NIR luminescent probes for time-gated biomedical imaging. *Nanoscale* **2020**, *12* (14), 7921–7926.
- (25) Robidillo, C. J. T.; Veinot, J. G. Functional bio-inorganic hybrids from silicon quantum dots and biological molecules. ACS Appl. Mater. Interfaces 2020, 12 (47), 52251–52270.
- (26) Erogbogbo, F.; Tien, C.-A.; Chang, C.-W.; Yong, K.-T.; Law, W.-C.; Ding, H.; Roy, I.; Swihart, M. T.; Prasad, P. N. Bioconjugation of luminescent silicon quantum dots for selective uptake by cancer cells. *Bioconjugate Chem.* **2011**, 22 (6), 1081–1088.
- (27) Zhai, Y.; Dasog, M.; Snitynsky, R. B.; Purkait, T. K.; Aghajamali, M.; Hahn, A. H.; Sturdy, C. B.; Lowary, T. L.; Veinot, J. G. Water-soluble photoluminescent D-mannose and L-alanine functionalized silicon nanocrystals and their application to cancer cell imaging. J. Mater. Chem. B 2014, 2 (47), 8427–8433.
- (28) Mangolini, L.; Kortshagen, U. Plasma-Assisted Synthesis of Silicon Nanocrystal Inks. *Adv. Mater.* **2007**, *19* (18), 2513–2519.
- (29) Anthony, R. J.; Cheng, K.-Y.; Holman, Z. C.; Holmes, R. J.; Kortshagen, U. R. An all-gas-phase approach for the fabrication of silicon nanocrystal light-emitting devices. *Nano Lett.* **2012**, *12* (6), 2822–2825.
- (30) Li, Z.; Kortshagen, U. R. Aerosol-phase synthesis and processing of luminescent silicon nanocrystals. *Chem. Mater.* **2019**, 31 (20), 8451–8458.
- (31) Kortshagen, U. R.; Sankaran, R. M.; Pereira, R. N.; Girshick, S. L.; Wu, J. J.; Aydil, E. S. Nonthermal plasma synthesis of nanocrystals: fundamental principles, materials, and applications. *Chem. Rev.* **2016**, *116* (18), 11061–11127.
- (32) Li, Z.; Robinson, Z. L.; Elvati, P.; Violi, A.; Kortshagen, U. R. Distance-dependent resonance energy transfer in alkyl-terminated Si nanocrystal solids. *J. Chem. Phys.* **2022**, *156* (12), 124705.
- (33) Mangolini, L.; Thimsen, E.; Kortshagen, U. High-yield plasma synthesis of luminescent silicon nanocrystals. *Nano Lett.* **2005**, *5* (4), 655–659
- (34) Holman, Z. C.; Kortshagen, U. R. A flexible method for depositing dense nanocrystal thin films: impaction of germanium nanocrystals. *Nanotechnology* **2010**, *21* (33), 335302.
- (35) Hessel, C. M.; Henderson, E. J.; Veinot, J. G. Hydrogen silsesquioxane: a molecular precursor for nanocrystalline Si– SiO2 composites and freestanding hydride-surface-terminated silicon nanoparticles. *Chem. Mater.* **2006**, *18* (26), 6139–6146.
- (36) Borchert, H.; Shevchenko, E. V.; Robert, A.; Mekis, I.; Kornowski, A.; Grübel, G.; Weller, H. Determination of nanocrystal sizes: a comparison of TEM, SAXS, and XRD studies of highly monodisperse CoPt3 particles. *Langmuir* 2005, 21 (5), 1931–1936.
- (37) Wang, Q.; Bao, Y.; Zhang, X.; Coxon, P. R.; Jayasooriya, U. A.; Chao, Y. Uptake and toxicity studies of poly-acrylic acid functionalized silicon nanoparticles in cultured mammalian cells. *Adv. Healthcare Mater.* **2012**, *1* (2), 189–198.
- (38) San Andrés, E.; Del Prado, A.; Mártil, I.; González-Díaz, G.; Bravo, D.; López, F. J.; Fernández, M.; Bohne, W.; Röhrich, J.; Selle, B.; et al. Bonding configuration and density of defects of SiO x H y thin films deposited by the electron cyclotron resonance plasma method. *J. Appl. Phys.* **2003**, *94* (12), 7462–7469.

- (39) Falcao, B. P.; Leitão, J. P.; Soares, M. R.; Ricardo, L.; Águas, H.; Martins, R.; Pereira, R. N. Oxidation and strain in free-standing silicon nanocrystals. *Phys. Rev. Appl.* **2019**, *11* (2), 024054.
- (40) Wu, J. J.; Kondeti, V. S. S. K.; Bruggeman, P. J.; Kortshagen, U. R. Luminescent, water-soluble silicon quantum dots via micro-plasma surface treatment. *J. Phys. D: Appl. Phys.* **2016**, 49 (8), 08LT02.
- (41) Loh, K. Q.; Andaraarachchi, H. P.; Ferry, V. E.; Kortshagen, U. R. Photoluminescent Si/SiO2 Core/Shell Quantum Dots Prepared by High-Pressure Water Vapor Annealing for Solar Concentrators, Light-Emitting Devices, and Bioimaging. ACS Appl. Nano Mater. 2023, 6 (7), 6444–6453.
- (42) Gelloz, B.; Juangsa, F. B.; Nozaki, T.; Asaka, K.; Koshida, N.; Jin, L. Si/SiO₂ core/shell luminescent silicon nanocrystals and porous silicon powders with high quantum yield, long lifetime, and good stability. *Front. Phys.* **2019**, *7*, 47.
- (43) Pavesi, L.; Ceschini, M. Stretched-exponential decay of the luminescence in porous silicon. *Phys. Rev. B* **1993**, 48 (23), 17625–17628.
- (44) Linnros, J.; Lalic, N.; Galeckas, A.; Grivickas, V. Analysis of the stretched exponential photoluminescence decay from nanometer-sized silicon crystals in SiO₂. *J. Appl. Phys.* **1999**, *86* (11), 6128–6134.
- (45) Huisken, F.; Ledoux, G.; Guillois, O.; Reynaud, C. Light-emitting silicon nanocrystals from laser pyrolysis. *Adv. Mater.* **2002**, 14 (24), 1861–1865.
- (46) Thiessen, A. N.; Zhang, L.; Oliynyk, A. O.; Yu, H.; O'Connor, K. M.; Meldrum, A.; Veinot, J. G. A tale of seemingly "Identical" silicon quantum dot families: structural insight into silicon quantum dot photoluminescence. *Chem. Mater.* **2020**, 32 (16), 6838–6846.
- (47) Greben, M.; Khoroshyy, P.; Valenta, J. Spectral dependencies of the stretched exponential dispersion factor and photoluminescence quantum yield as a common feature of nanocrystalline Si. *Phys. Status Solidi A* **2020**, 217 (4), 1900698.
- (48) Bywalez, R.; Karacuban, H.; Nienhaus, H.; Schulz, C.; Wiggers, H. Stabilization of mid-sized silicon nanoparticles by functionalization with acrylic acid. *Nanoscale Res. Lett.* **2012**, *7*, 76.
- (49) Oh, E.; Liu, R.; Nel, A.; Gemill, K. B.; Bilal, M.; Cohen, Y.; Medintz, I. L. Meta-analysis of cellular toxicity for cadmium-containing quantum dots. *Nat. Nanotechnol.* **2016**, *11* (5), 479–486.
- (50) Özbilgin, İ. N. G.; Yamazaki, T.; Watanabe, J.; Sun, H.-T.; Hanagata, N.; Shirahata, N. Water-soluble silicon quantum dots toward fluorescence-guided photothermal nanotherapy. *Langmuir* **2022**, *38* (17), 5188–5196.
- (51) Gouget-Laemmel, A.; Yang, J.; Lodhi, M.; Siriwardena, A.; Aureau, D.; Boukherroub, R.; Chazalviel, J.-N.; Ozanam, F.; Szunerits, S. Functionalization of azide-terminated silicon surfaces with glycans using click chemistry: XPS and FTIR study. *J. Phys. Chem.* C **2013**, 117 (1), 368–375.